JCI insight

Monocyte glycolysis determines CD8+ T cell functionality in human Chagas disease

Liliana María Sanmarco, Natalia Eberhardt, Gastón Bergero, Luz Piedad Quebrada Palacio, Pamela Martino Adami, Laura Marina Visconti, Ángel Ramón Minguez, Yolanda Hernández-Vasquez, Eugenio Antonio Carrera Silva, Laura Morelli, Miriam Postan, Maria Pilar Aoki

Research Article   Immunology   Metabolism

Chagas disease is a lifelong pathology resulting from *Trypanosoma cruzi* infection. It represents one of the most frequent causes of heart failure and sudden death in Latin America. Herein, we provide evidence that aerobic glycolytic pathway activation in monocytes drives nitric oxide (NO) production, triggering tyrosine nitration (TN) on CD8+ T cells and dysfunction in patients with chronic Chagas disease. Monocytes from patients exhibited a higher frequency of hypoxia-inducible factor 1α and increased expression of its target genes/proteins. Nonclassical monocytes are expanded in patients' peripheral blood and represent an important source of NO. Monocytes entail CD8+ T cell surface nitration because both the frequency of nonclassical monocytes and that of NO-producing monocytes positively correlated with the percentage of TN+ lymphocytes. Inhibition of glycolysis in in vitro–infected peripheral blood mononuclear cells decreased the inflammatory properties of monocytes/macrophages, diminishing the frequency of IL-1β– and NO-producing cells. In agreement, glycolysis inhibition reduced the percentage of TN+CD8+ T cells, improving their functionality. Altogether, these results clearly show that glycolysis governs oxidative stress on monocytes and modulates monocyte–T cell interplay in human chronic Chagas disease. Understanding the pathological immune mechanisms that sustain an inflammatory environment in human pathology is key to designing improved therapies.

Find the latest version:

https://jci.me/123490/pdf

JCI insight

Monocyte glycolysis determines CD8+ T cell functionality in human Chagas disease

Liliana María Sanmarco,[1,2] Natalia Eberhardt,[1,2] Gastón Bergero,[1,2] Luz Piedad Quebrada Palacio,[3] Pamela Martino Adami,[4,5] Laura Marina Visconti,[6,7] Ángel Ramón Minguez,[6] Yolanda Hernández-Vasquez,[3] Eugenio Antonio Carrera Silva,[8] Laura Morelli,[4,5] Miriam Postan,[3] and Maria Pilar Aoki[1,2]

[1]Universidad Nacional de Córdoba, Facultad de Ciencias Químicas, Departamento de Bioquímica Clínica, Córdoba, Argentina. [2]Consejo Nacional de Investigaciones Científicas y Tecnológicas (CONICET), Centro de Investigaciones en Bioquímica Clínica e Inmunología (CIBICI), Córdoba, Argentina. [3]Instituto Nacional de Parasitología "Dr. Mario Fatala Chabén," Buenos Aires, Argentina. [4]Laboratorio de Amiloidosis y Neurodegeneración, Fundación Instituto Leloir, Buenos Aires, Argentina. [5]Instituto de Investigaciones Bioquímicas de Buenos Aires, Consejo Nacional de Investigaciones Científicas y Técnicas (CONICET), Buenos Aires, Argentina. [6]Hospital Nuestra Señora de la Misericordia, Córdoba, Argentina. [7]Universidad Nacional de Córdoba, Facultad de Ciencias Médicas, II Cátedra de Infectología, Córdoba, Argentina. [8]Laboratorio de Trombosis Experimental, Instituto de Medicina Experimental, Academia Nacional de Medicina, CONICET, Buenos Aires, Argentina.

Chagas disease is a lifelong pathology resulting from *Trypanosoma cruzi* infection. It represents one of the most frequent causes of heart failure and sudden death in Latin America. Herein, we provide evidence that aerobic glycolytic pathway activation in monocytes drives nitric oxide (NO) production, triggering tyrosine nitration (TN) on CD8+ T cells and dysfunction in patients with chronic Chagas disease. Monocytes from patients exhibited a higher frequency of hypoxia-inducible factor 1α and increased expression of its target genes/proteins. Nonclassical monocytes are expanded in patients' peripheral blood and represent an important source of NO. Monocytes entail CD8+ T cell surface nitration because both the frequency of nonclassical monocytes and that of NO-producing monocytes positively correlated with the percentage of TN+ lymphocytes. Inhibition of glycolysis in in vitro–infected peripheral blood mononuclear cells decreased the inflammatory properties of monocytes/macrophages, diminishing the frequency of IL-1β– and NO-producing cells. In agreement, glycolysis inhibition reduced the percentage of TN+CD8+ T cells, improving their functionality. Altogether, these results clearly show that glycolysis governs oxidative stress on monocytes and modulates monocyte–T cell interplay in human chronic Chagas disease. Understanding the pathological immune mechanisms that sustain an inflammatory environment in human pathology is key to designing improved therapies.

Introduction

Monocytes are critical components not only of the innate immune system but also of adaptive immune response development. Based on the relative surface expression of LPS coreceptor CD14 and of FcγIII receptor CD16, they have been classified into 3 subtypes: "classical monocytes" (CD14++CD16−), "nonclassical monocytes" (CD14+CD16++), and "intermediate monocytes" (CD14++CD16+) (1, 2). So far, however, there is poor understanding of the effector functions of each monocyte subset and numerous reports show contradictory results (3).

Under hypoxic or inflammatory conditions, monocytes activate transcriptional responses, which are governed by the transcription factor hypoxia-inducible factor 1α (HIF-1α). The accumulation of HIF-1α protein requires the metabolism of glucose into pyruvate that prevents the aerobic degradation of HIF-1α protein. HIF-1α target genes include glucose transporters GLUT-1 and GLUT-3 (4–6). Glucose can be used throughout 2 integrated pathways, the first of which, the glycolytic pathway, involves the cytoplasmic conversion of glucose into pyruvate, with the consequent generation of 2 ATP molecules and, in anaerobic conditions, lactate. Extracellular ATP (eATP) and lactate activate HIF-1α (7, 8), thus resulting in a positive feedback loop. The second pathway, the tricarboxylic acid cycle, generates the reducing equivalents nicotinamide adenine

dinucleotide (NADH) and flavin adenine dinucleotide, which donate electrons to the electron transport chain to fuel oxidative phosphorylation (OXPHOS), the process by which 32 ATP molecules are generated in the mitochondria.

In inflammatory settings, OXPHOS is inhibited by nitric oxide (NO) production in monocyte-derived inflammatory dendritic cells (moDCs) in an autocrine manner. In the absence of an active respiratory chain, sustained glycolytic metabolism is essential for moDC survival and function (9). Furthermore, NO production seems to be central in orchestrating HIF-1α responses by inducing its stabilization and transcriptional activation (10).

Chagas disease, a complex pathological condition resulting from *Trypanosoma cruzi* infection, has become one of the most frequent causes of heart failure, cardio-embolic stroke, and sudden death in Latin America (11). The acute phase lasts 2–3 months and is characterized by detectable parasitemia and active parasite replication within target tissues. However, clinical symptoms are usually mild and nonspecific, and the vast majority of acute infections are never detected. During this phase, cell-mediated immunity controls parasite levels, but it is insufficient to completely clear the infection; most individuals remain infected for life. People who survive the acute phase enter a chronic asymptomatic phase (indeterminate stage), which is generally symptomless and may last from 10 to 30 years. Approximately 30% of patients in this period, also recognized as "silent," may develop heart abnormalities (12) that could give rise to the cardiac form of chronic infection. Although antiparasitic therapy is clearly recommended for acute Chagas disease, the treatment of patients in the chronic stage is controversial. This is largely due to a lack of large, randomized trials and incomplete understanding of pathological immune mechanisms developed during this stage. After decades of controversies, it is widely accepted nowadays that parasite persistence is a necessary and sufficient condition for the sustained inflammatory responses underlying the progression of cardiac lesions of chronic Chagas disease (13–18). Thus, one of the main challenges in understanding Chagas myocarditis immunopathology is to find out why, despite a robust immune response during the acute phase of the infection, the parasite is not completely eliminated, being able to sustain a pathological inflammatory environment.

Cell-mediated immunity involves activation of phagocytes and of cytotoxic T lymphocytes (CTLs). In this sense, we have recently reported increased IL-1β plasma levels concomitant with enhanced frequency of NO-producing leukocytes and the surface nitration of CTLs associated with decreased functionality of this T cell compartment in the peripheral blood from patients with Chagas disease in the indeterminate phase (19). In this study, we went deeper by exploring how metabolism affects the monocyte compartment and T cell functionality during this human infectious disease. We have found that the nonclassical monocyte subpopulation expanded in the peripheral blood of both asymptomatic and symptomatic chronic Chagas disease patients, with this subpopulation being an important source of NO production. Additionally, total monocytes from patients with Chagas disease exhibited higher HIF-1α expression, glucose uptake, and glycolytic activity relative to control donors. In agreement, glycolysis inhibition decreased IL-1β and NO production in *T. cruzi*–infected peripheral blood mononuclear cell (PBMC) cultures and diminished T cell nitration. Thus, the CTL dysfunction observed in infected individuals is associated with the metabolic pathway activated in the monocyte compartment.

Results

Patients with Chagas disease have increased frequencies of NO+ and HIF-1α+ monocytes. Peripheral blood samples from 40 patients with Chagas disease and 55 from control donors of both sexes were collected and tested for *T. cruzi*–specific antibodies by ELISA and indirect hemagglutination (IHA) (Table 1). The median value for anti–*T. cruzi* antibody titer was 1/256 (local cutoff titer 1/32) detected by IHA. Patients were grouped according to Kuschnir classification (20): 88% (35/40) of patients were grouped into group 0 (G0), 10% (4/40) into group 1 (G1), and 2% (1/40) into group 3 (G3).

To identify the main cellular source of NO from circulating leukocytes, we measured NO production in polymorphonuclear cells (PMNCs) and monocytes by flow cytometry following the gating strategy depicted in Figure 1A. Patients with Chagas disease exhibited higher frequency of NO-producing monocytes, but no differences were detected in the percentage of NO-producing PMNCs relative to control donors (Figure 1B). Furthermore, the production of ROS by monocytes and PMNCs was similar between both groups (Supplemental Figure 1; supplemental material available online with this article; https://doi.org/10.1172/jci.insight.123490DS1). Notably, no significant differences were found in the percentages of NO- and ROS-producing monocytes comparing patients in the asymptomatic phase (G0) versus symptomatic patients (G1

Table 1. Demographic and clinical data

	Control donors (CON) *n* = 55	Chagas disease patients (CHAG) *n* = 40
Age (years old)		
Range	19–60	20–60
Median	31	35
Sex		
Female	*n* = 37	*n* = 30
Male	*n* = 18	*n* = 10
Clinical evaluation		
Electrocardiographic changes	NE	*n* = 5
Echocardiographic changes	NE	*n* = 5
Chest x-ray abnormalities	NE	*n* = 1

NE, not evaluated.

and G3) (P = 0.83 and P > 0.99, respectively). Because NO production results from inducible NO synthase (iNOS) activity and this enzyme is an HIF-1α target molecule, we evaluated HIF-1α protein expression in the monocyte population by flow cytometry. We have found that patients with Chagas disease exhibited increased frequency of HIF-1α+ monocytes in comparison with control donors, although the molecular expression levels per cell (MFI) remained unchanged (Figure 1C).

Despite the fact that hypoxia could activate an inflammatory response, HIF-1α activation leads to increased extracellular adenosine production as an essential endogenous antiinflammatory mediator to protect from tissue damage (21). Adenosine is originated from the sequential dephosphorylation of eATP, mainly by the subsequent action of CD39 and CD73 ectoenzymes (22, 23). In line with this, we observed increased plasmatic ATP levels (Figure 1D), associated with higher frequency of circulating monocytes expressing CD39 in *T. cruzi*–infected patients compared with control donors, but we found similar expression of this ectoenzyme per cell (MFI) in both studied groups (Figure 1E). Although we did not observe differences in the percentage of CD73+ monocytes, interestingly, a higher MFI of this enzyme was detected in monocytes from seropositive patients (Figure 1F).

Monocytes from T. cruzi–infected patients exhibit increased functional activity. Following the gating strategy described in Figure 2A, we found that monocytes from patients showed increased frequency of IL-1β, IL-6, and IL-10 production compared with control donors in response to in vitro stimulation with the proinflammatory stimulus (LPS). Moreover, the amounts of IL-1β and IL-6 (measured as MFI) were also significantly increased in monocytes from *T. cruzi*–infected patients, but no differences were observed in IL-10 levels (Figure 2B). Strikingly, under parasite lysate stimulation, intracellular production of IL-6 and IL-1β was higher in monocytes from patients than the control counterpart (Figure 2C).

The monocyte subpopulations were defined by the expression of CD14 and/or CD16 (Figure 3A). The percentage of circulating CD14++CD16− (classical) monocytes decreased, while the frequency of CD14+CD16++ (nonclassical) subset increased in seropositive patients when compared with control donors (Figure 3B) as was observed for bacterial and viral infections (24–26). The percentages of NO- and ROS-producing monocytes were significantly higher in the nonclassical monocyte subset than in the classical monocyte subpopulation in both groups, patients and control donors (Figure 3, C and D). Conversely, the proportion of nonclassical monocytes producing IL-10 or IL-6 was lower than the frequency of IL-10+/IL-6+ classical monocytes (Figure 3, E and F) in both studied groups. We found no differences in the frequency of nonclassical monocytes from asymptomatic patients (G0) and from those in the cardiac chronic stage (G1 and G3) (P > 0.99). Altogether, the results clearly demonstrate that the nonclassical subset of monocytes displays prooxidative properties.

Strikingly, Glut-1 expression exhibited a dichotomic pattern in classical and nonclassical monocyte subsets between both groups. In seropositive patients, nonclassical monocytes exhibited increased Glut-1 expression while the main Glut-1+ subset in healthy control was classical monocytes (Figure 3G). Although CD39 expression did not show a significant difference in both monocyte subpopulations (Figure 3H), increased CD73 expression was detected in nonclassical monocytes in comparison with classical monocytes, in control as well as in patient samples (Figure 3I).
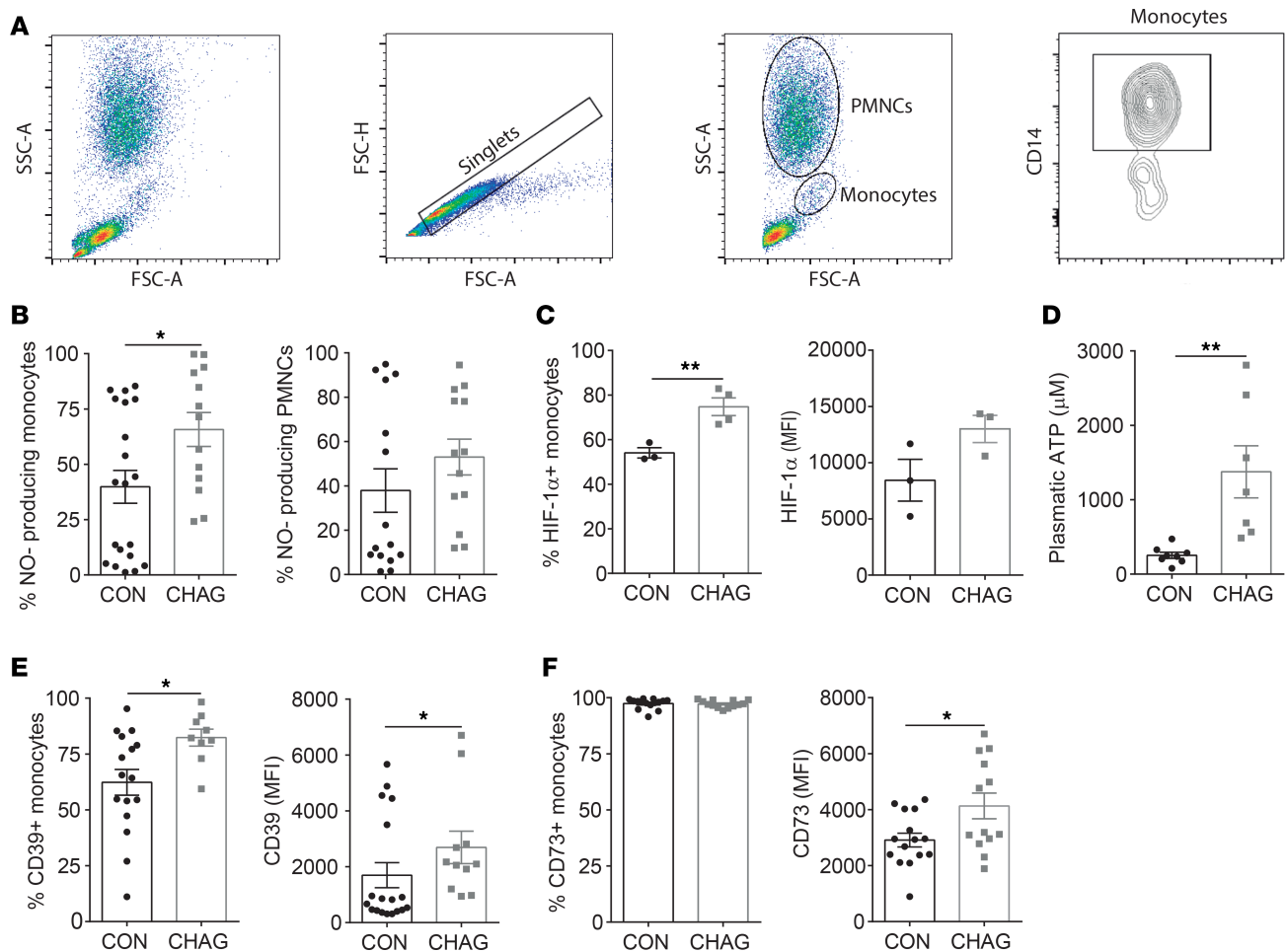
Figure 1. Patients with Chagas disease show increased frequency of NO⁺ and HIF-1α⁺ monocytes. (**A**) Flow cytometry gating strategy for leukocytes from peripheral blood samples. After exclusion of doublets and debris by using forward light scatter–height (FSC-H) versus forward light scatter–area (FSC-A) density dot plots, polymorphonuclear cells (PMNCs) and monocytes were gated according to their FSC-A versus SSC-A features. Monocytes were further identified by CD14⁺ staining. (**B**) Frequency of NO-producing circulating monocytes and PMNCs from control donors (CON; n = 20) and Chagas patients (CHAG; n = 13). (**C**) Frequency and MFI of HIF-1α⁺ monocytes from CHAG (n = 4) and CON (n = 4). (**D**) ATP levels in plasma from CON (n = 8) and CHAG (n = 8). Frequency and MFI of (**E**) CD39⁺ and (**F**) CD73⁺ monocytes from CON (n = 16) and CHAG (n = 13). Data are presented as mean ± SEM. *P < 0.05; **P < 0.01 (Student's t test or Mann-Whitney U test).

Monocytes from T. cruzi–infected patients showed increased glycolysis and mitochondrial damage. HIF-1α drives multiple immune cell effector functions, including energy metabolism. Indeed, the HIF-1α–dependent glycolytic pathway orchestrates a metabolic checkpoint for the differentiation of the Th17 profile (27), type 1 Treg (Tr1) cells (28), and classically activated macrophages (29). To determine whether monocytes from patients with Chagas disease have enhanced glycolytic metabolism, we measured extracellular acidification rate (ECAR), and oxygen consumption rate (OCR), as measures of glycolysis and OXPHOS, respectively.

Higher glycolysis, glycolytic capacity, and glycolytic reserve were observed in monocytes from seropositive patients compared with control donors (Figure 4, A and B). Consistent with these findings, *T. cruzi*–infected patients exhibited higher frequency of Glut-1⁺ monocytes relative to controls (Figure 4C). Of note, monocytes from asymptomatic (G0), seropositive individuals did not exhibit differences in glycolytic activity compared to monocytes from patients in cardiac chronic G1 and G3 stages (*P* > 0.99 glycolytic activity).

Moreover, monocytes from patients showed lower respiration driving ATP synthesis and OCR and higher respiration driving proton leak in comparison with control donors (Figure 4, D and E). Consequently, monocytes from infected individuals exhibited a significant decrease in the Bioenergetic Health Index (BHI), a proposed functional biomarker of oxidative stress in patients suffering metabolic disorders (ref. 30 and Figure 4F). To distinguish between mitochondria with altered or unaltered mitochondrial potential (31), we stained monocytes with a combination of MitoTracker Green (Δψ-independent mitochondrial stain) and
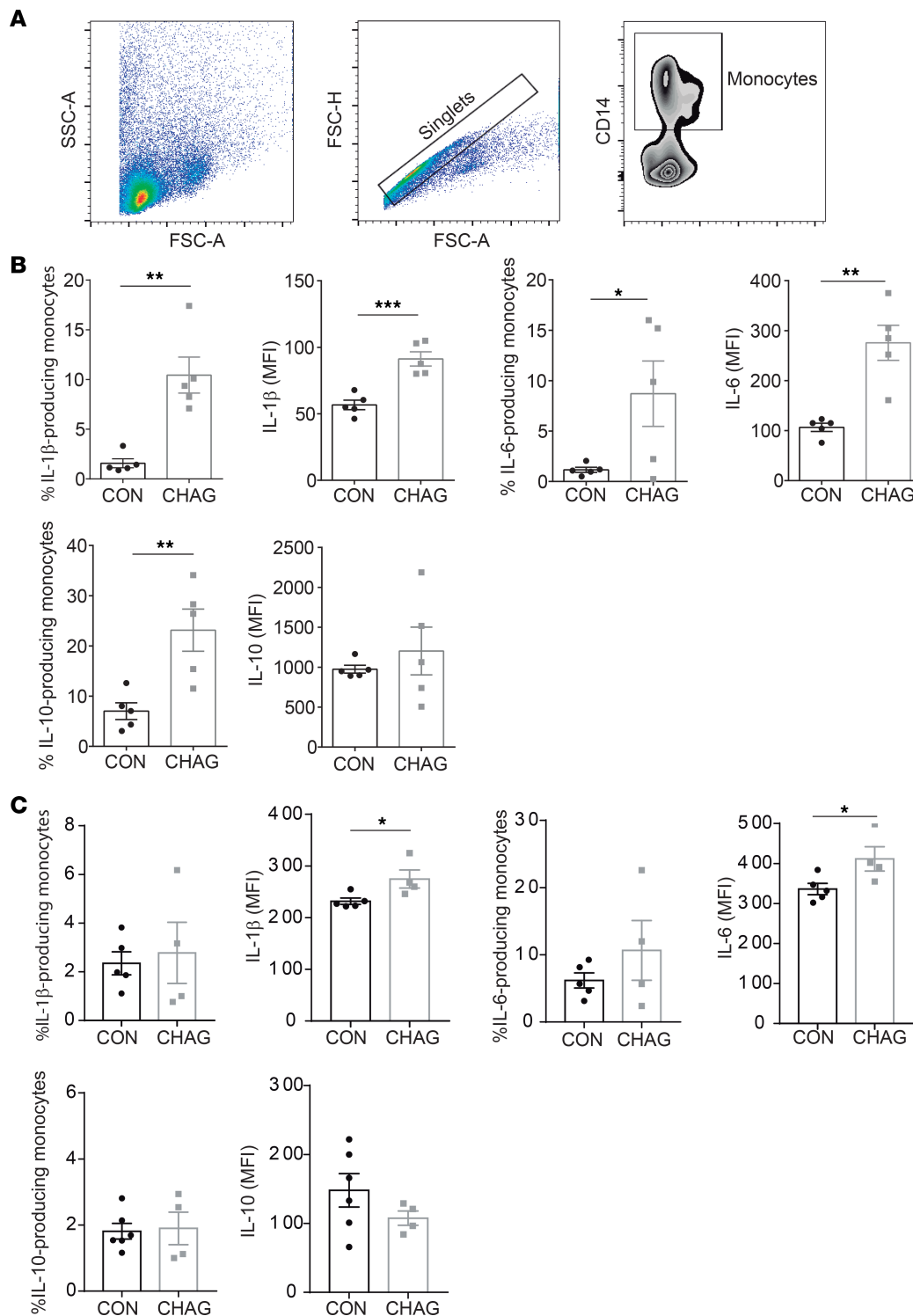
Figure 2. Monocytes from *T.cruzi*–infected patients exhibit higher functional activity potential. (**A**) For intracellular cytokine analysis, PBMCs isolated from peripheral blood from control donors and from seropositive patients were cultured with monensin, brefeldin A, and (**B**) LPS (CON, *n* = 5; CHAG, *n* = 5) or (**C**) parasite lysate (CON, *n* = 6; CHAG, *n* = 4) and stained with anti-CD14-PE-Cy5. After staining of surface markers, cells were fixed and made permeable. Then the cells were stained with anti-IL-1β, anti-IL-6, and anti-IL-10 antibodies and analyzed by flow cytometry. PBMCs were gated according to their CD14+ staining after exclusion of doublets and debris by using FSC-H/FSC-A dot plots. Frequency and MFI of IL-1β–, IL-6–, and IL-10–producing monocytes. Data are presented as mean ± SEM. *$P <$ 0.05; **$P <$ 0.01; ***$P <$ 0.001 (Student's *t* test or Mann-Whitney *U* test).

MitoTracker Orange (Δψ-dependent mitochondrial stain). A marked increase in the number of dysfunctional mitochondria (MitoTracker Green[hi], MitoTracker Orange[lo]) and in mitochondrial mass (MitoTracker Green staining) was found in monocytes from seropositive patients compared with monocytes from control donors (Figure 4G).

Monocyte glycolysis is necessary for T. cruzi–induced lymphocyte nitration and dysfunction. Because glycolytic activity has been extensively associated with proinflammatory activities of immune cells, we characterized the effect of glycolysis on monocyte effector function during *T. cruzi* infection. To this aim, in vitro–infected PBMCs were pretreated with a synthetic glucose analog, 2-DG, that inhibits
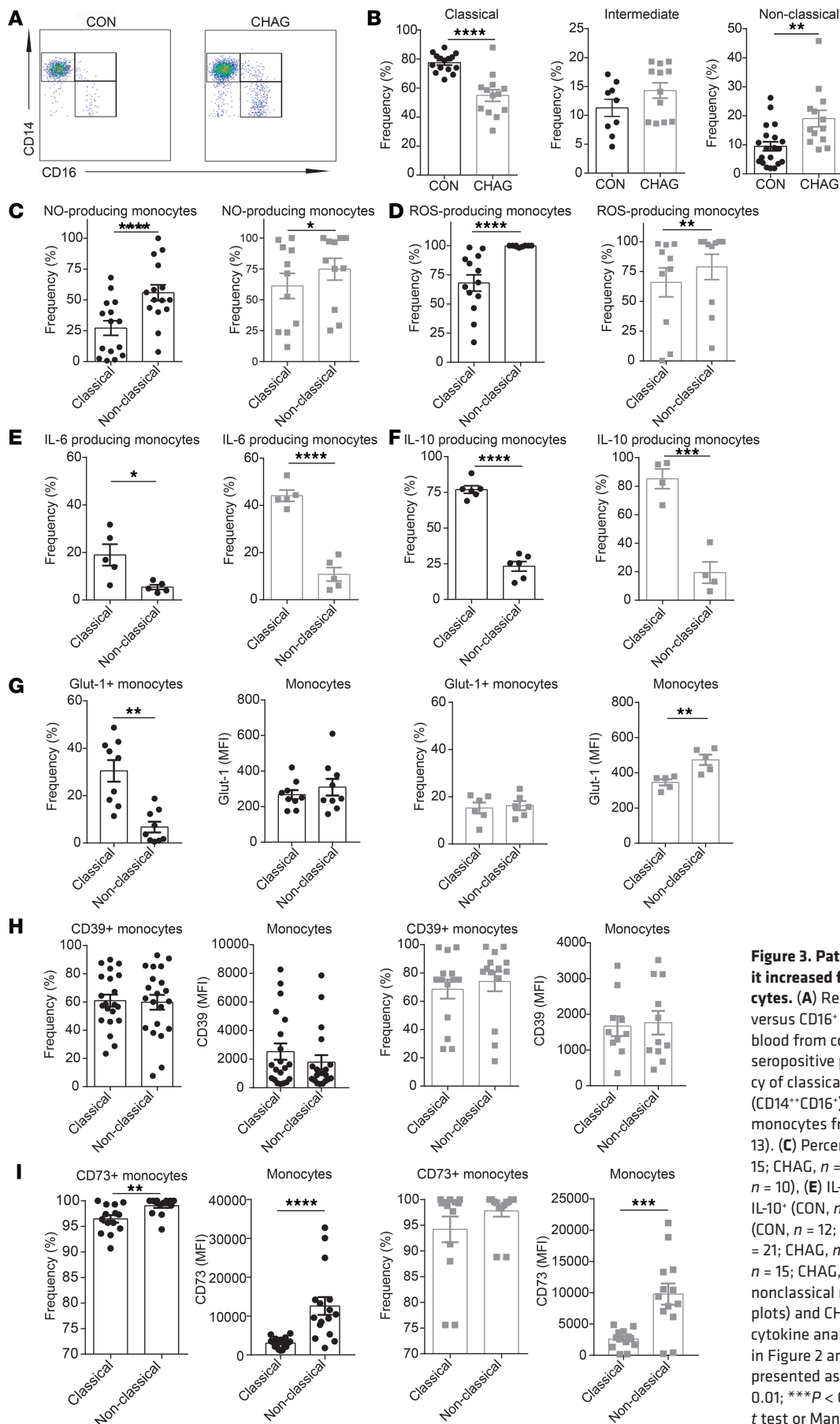
Figure 3. Patients with Chagas disease exhibit increased frequency of nonclassical monocytes. (A) Representative dot plots of CD14⁺ versus CD16⁺ monocyte subsets in peripheral blood from control donors (CON) and from seropositive patients (CHAG). (B) Frequency of classical (CD14⁺⁺CD16⁻), intermediate (CD14⁺⁺CD16⁺), and nonclassical (CD14⁺CD16⁺⁺) monocytes from CON ($n = 20$) and CHAG ($n = 13$). (C) Percentage and MFI of NO⁺ (CON, $n = 15$; CHAG, $n = 11$), (D) ROS⁺ (CON, $n = 13$; CHAG, $n = 10$), (E) IL-6⁺ (CON, $n = 5$; CHAG, $n = 5$), (F) IL-10⁺ (CON, $n = 5$; CHAG, $n = 5$), (G) Glut-1⁺ (CON, $n = 12$; CHAG, $n = 6$), (H) CD39⁺ (CON, $n = 21$; CHAG, $n = 14$), and (I) CD73⁺ cells (CON, $n = 15$; CHAG, $n = 15$) gated in classical versus nonclassical monocytes from CON (black plots) and CHAG (gray plots). For intracellular cytokine analysis, the cells were processed as in Figure 2 and stimulated with LPS. Data are presented as mean ± SEM. *$P < 0.05$; **$P < 0.01$; ***$P < 0.001$; ****$P < 0.0001$ (Student's t test or Mann-Whitney U test).
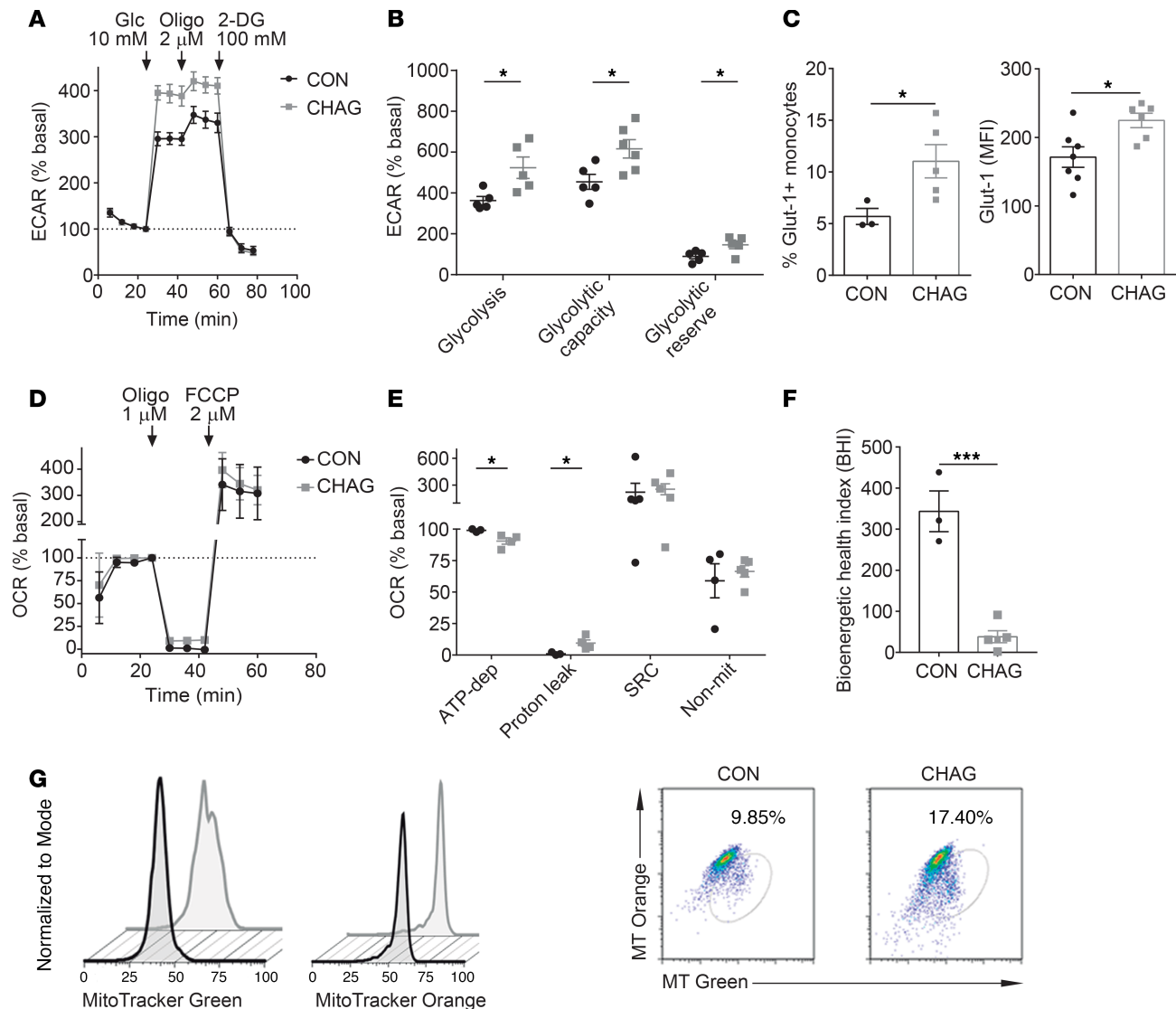
Figure 4. Monocytes from *T.cruzi*–infected patients show increased glycolysis and altered mitochondrial potential. (A) Monocytes from control donors (CON) or patients with Chagas disease (CHAG) isolated by CD14+ selection were seeded in a Seahorse XFp analyzer, and real-time extracellular acidification rate (ECAR) was determined during sequential treatments with glucose, oligomycin (ATP synthase inhibitor) and 2-deoxyglucose (2-DG) (glycolysis inhibitor). Data represent mean ± SEM of 8 runs. **(B)** Bars show glycolytic rate, glycolytic capacity, and glycolytic reserve of monocytes from CON ($n = 5$) and CHAG ($n = 5$). To analyze these parameters, first nonglycolytic acidification was subtracted, and then the data were normalized to basal ECAR. **(C)** Frequency and MFI of Glut-1+ monocytes from CON ($n = 3$) and CHAG ($n = 5$). **(D)** Real-time mitochondrial respiration was analyzed starting from basal respiration and after the addition of oligomycin (complex V inhibition), FCCP (maximal respiration induction), and rotenone/antimycin A mixture (electron transport chain inhibition). Data represent mean ± SEM of 5 experiments. Bars show **(E)** respiration driving ATP synthesis, respiration driving proton leak, spare respiratory capacity, nonmitochondrial OCR, and **(F)** Bioenergetic Health Index (BHI) of monocytes from CON ($n = 4$) and CHAG ($n = 5$). To analyze these parameters, first nonmitochondrial OCR was subtracted, and then the data were normalized to basal OCR. **(G)** Representative histogram of total mitochondrial mass analyzed by flow cytometry in monocytes from CON (black line) and CHAG (gray line) labeled with MitoTracker Green. Mitochondrial membrane potential was analyzed in monocytes from CON (black line) and CHAG (gray line) labeled with MitoTracker Orange. Representative dot plot of mitochondrial mass versus mitochondrial membrane potential in CON ($n = 3$) and CHAG ($n = 5$) monocytes. Data are presented as mean ± SEM. *$P < 0.05$; ***$P < 0.001$ (Student's t test or Mann-Whitney U test).

glycolysis and compared with untreated infected PBMCs from the same donor. We found that 2-DG treatment did not modify M1 marker (CD64) expression but increased M2 marker mannose receptor (CD206) expression on infected monocytes/macrophages (Mo/Ma) (Figure 5A). Moreover, glycolysis inhibition decreased the frequency of IL-6– and of IL-1β–producing Mo/Ma, as well as the amount of IL-1β released to the culture supernatant (Figure 5, B and C). In contrast, glycolysis inhibition raised the percentage of IL-10–producing Mo/Ma (Figure 5D).
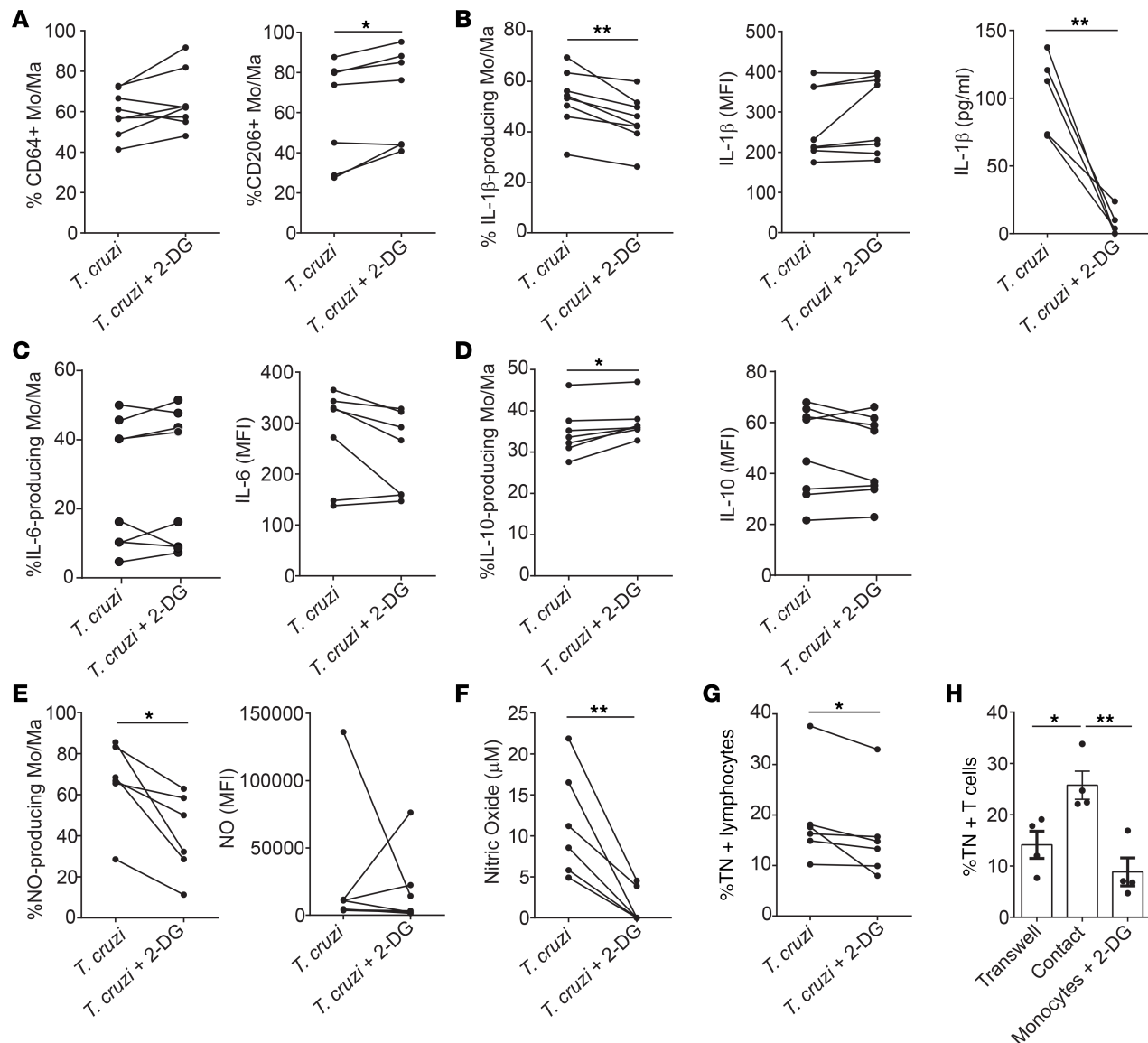
Figure 5. Glycolytic activity inhibition decreases NO-producing monocytes and lymphocyte nitration induced by *T. cruzi* infection. Infected PBMCs from control donors (*n* = 8) were treated or not with 2-DG. (**A**) Frequency of CD64+ and CD206+ monocytes/macrophages (Mo/Ma). (**B**) Percentage and MFI of IL-1β+ Mo/Ma (left) and IL-1β levels in culture supernatants measured by ELISA (right). (**C**) Percentage and MFI of IL-6+, (**D**) IL-10+, and (**E**) NO+ Mo/Ma. (**F**) NO levels measured in culture supernatants by Griess reaction. (**G**) Frequency of TN+CD3+ lymphocytes. *$P < 0.05$; **$P < 0.01$ (paired Student's *t* test or Wilcoxon's test). (**H**) Infected purified monocytes from control donors (buffy coat) were cultured with purified lymphocytes in independent chambers (Transwell) or in the same chamber (contact); in some cocultures, monocytes were treated with 2-DG (monocytes + 2DG) (2-way ANOVA with post hoc Tukey's) (representative experiment, *n* = 4; from 2 independent experiments). TN, tyrosine nitration.

To evaluate the effect of monocyte glycolysis on T cell nitration, we measured NO production and tyrosine nitration–positive (TN+) lymphocytes in infected PBMC cultures subjected to 2-DG treatment. The glucose analog lowered the frequency of NO-producing Mo/Ma (Figure 5E), NO levels in culture supernatant (Figure 5F), as well as the frequency of T cell nitration (Figure 5G). To further define the link between monocyte glycolytic metabolism and T cell nitration, in vitro–infected monocytes were pretreated with 2-DG. After 3 hours, the monolayers were washed and cocultured with sorted CD3+ lymphocytes. The inhibition of glycolysis decreased the percentage of TN+ T cells (Figure 5H). Furthermore, T cell nitration was cell contact dependent because the disruption of physical contact between infected monocytes and T cells abrogated the nitration of lymphocytes (Figure 5H).

To confirm that NO production by monocytes induces CTL dysfunction during *T. cruzi* infection, we treated PBMCs from control donors with NO production inhibitor L-NAME previous to infection. We observed that
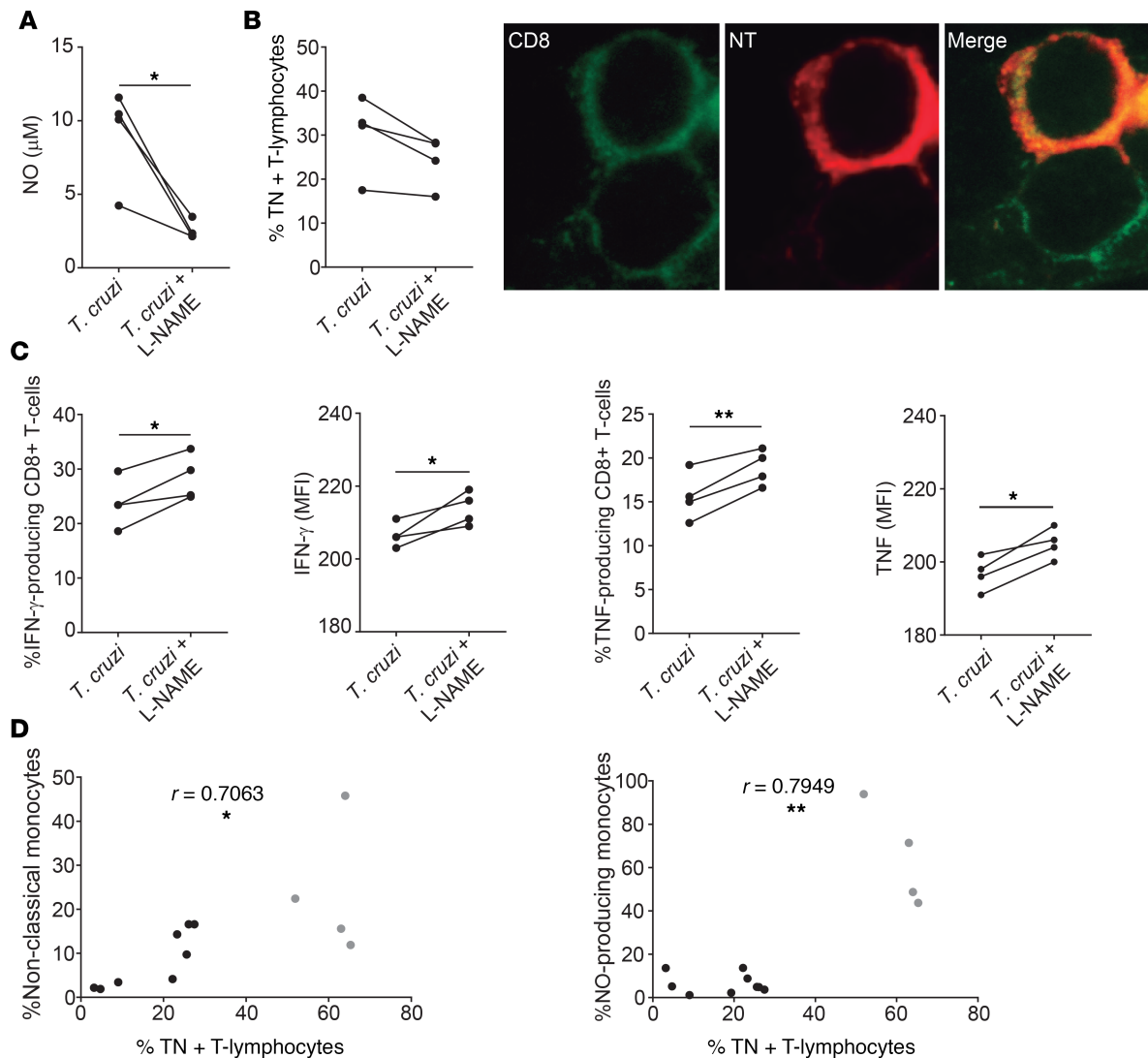
Figure 6. NO production drives TN on CTLs' surface and CD8⁺ T cell dysfunction. Infected PBMCs from control donors (*n* = 4) were treated or not with L-NAME. (**A**) NO levels in culture supernatants measured by Griess reaction. (**B**) Frequency of TN⁺CD3⁺ lymphocytes (left) and representative images of cells from seropositive patient peripheral blood labeled with anti-TN antibody (red) and anti-CD8 antibody (green) (original magnification, ×1000) (right). (**C**) Percentage and MFI of IFN-γ⁺ and TNF⁺ cells also positive for CD8 and CD3 expression. *$P < 0.05$; **$P < 0.01$ (paired Student's *t* test or Wilcoxon's test). (**D**) Pearson's correlation analysis between the percentage of TN⁺CD3⁺ lymphocytes versus the frequency of nonclassical monocytes (left) and between the percentage of TN⁺CD3⁺ lymphocytes versus the frequency of NO-producing monocytes (right) from control donors (black dots; *n* = 8) and from seropositive patients (gray dots; *n* = 4). TN, tyrosine nitration.

L-NAME reduced NO levels (Figure 6A) and lymphocyte nitration (Figure 6B) and reestablished the effector function as measured by IFN-γ and TNF production by CTLs (Figure 6C) compared with untreated infected cells. Altogether, these results clearly evidence that glycolysis governs oxidative stress on monocytes and consequently regulates T cell function in the context of *T. cruzi* infection.

Our hypothesis was further confirmed by the fact that both the frequency of nonclassical monocytes and the frequency of NO-producing monocytes positively correlated with the percentage of TN⁺ lymphocytes in peripheral blood samples from *T. cruzi*–infected patients and control donors (Figure 6D).

Discussion

Monocytes are key players in antiparasitic immune response because they produce inflammatory cytokines, inflammation-accelerating chemokines, and microbicidal species. The present study demonstrates that during human chronic *T. cruzi* infection, monocytes exhibit long-lasting functional phenotypic changes because they are more prone to produce cytokines under stimulation, and they exhibited increased production of NO

compared with monocytes from control donors, contrasting with the impaired effector function of the CTL compartment (19). Cytotoxic CD8+ T cells from seropositive patients are more susceptible to apoptosis and exhibit high levels of nitrated tyrosine residues on their surface. Naive cells constitute the main subpopulation that undergoes TN. Notably, TN+ CTLs are less functional than the TN− population because TN+ CTLs exhibit deactivation of the cytotoxic function with lower expression of CD107a (a degranulation marker) and decreased production of cytokines (IFN-γ, TNF, and IL-2). The nitration of surface proteins on T cells is promoted by peroxynitrites, which are induced by the reaction of NO with the superoxide anion (32–34). In the present work, we identified nonclassical monocytes as an important cellular source of NO, which promotes CD8+ T cell nitration/dysfunction in this human infectious disease.

The expanded nonclassical monocyte subset has been previously described in the context of different inflammation-related diseases (35–37). Regarding Chagas disease, our results are in full agreement with a recent report from Pérez-Mazliah's group. The authors found that *T. cruzi*–infected patients with mild or no signs of cardiac disease exhibited increased levels of nonclassical monocytes in comparison with control donors (38).

In the present work, we have also found increased monocyte-expressing HIF-1α, a transcription factor that could be promoting the enhanced amount of plasmatic IL-1β observed in patients with Chagas disease (19). In fact, it was recently demonstrated that activated macrophages produce IL-1β because of HIF-1α stabilization in a mechanism supported by glycolysis (29). The metabolism of glucose into pyruvate prevents aerobic degradation of HIF-1 protein, allowing HIF-1 accumulation. Accordingly, total monocytes isolated from patients showed activated glycolytic metabolism in comparison with their control counterpart.

HIF-1 is the master regulator of metabolic adaptation to hypoxia with a broad range of effector functions. Among these, NO production is a recognized downstream effect of HIF-1α because this transcription factor stimulates the expression of iNOS. Interestingly, although *T. cruzi*–infected patients exhibited higher frequency of NO-producing monocytes, this mediator is not augmented in plasma from infected patients (19), which is consistent with data from the literature (39). Regarding cellular NO effector functions, Everts and coworkers demonstrated an autocrine NO effect on dendritic cell metabolism (9). They postulated the notion that NO inhibits mitochondrial electron transport by the nitrosylation of iron sulfur–containing proteins from complex I (NADH-ubiquinone oxidoreductase), complex II (succinate-ubiquinone oxidoreductase), and complex IV (cytochrome *c* oxidase), thereby blocking oxygen consumption and ATP production (40–42). The direct connection between reduced respiratory rate and inflammation has been recognized for some time (43). In this sense, cells with mitochondrial damage activate the glycolytic metabolism to produce the ATP necessary to survive. Our results suggest that oxidative stress disrupts mitochondrial potential in monocytes from seropositive individuals. In turn, these cells enhance the activation of glycolytic metabolism supporting their inflammatory state.

Mitochondria are subcellular organelles that play vital roles in the eukaryotic cells. Even though their function in energy metabolism is extensively recognized, only a few years ago, several studies demonstrated the relevance of mitochondria in immunity as a platform for immune regulation (29, 44–48). Mitochondrial function could be assessed by respiration driving ATP production, respiration driving proton leak, maximal respiration, and spare respiratory capacity, among others. Each of these parameters is sensitive to different free radicals or oxidants, clearly indicating that mitochondria are particularly susceptible to oxidative stress. In agreement with our results, a high percentage of cardiac and skeletal muscle mitochondria exhibiting structural and functional alterations was reported in patients with Chagas disease, even in those without clinical criteria of cardiomyopathy (49, 50). In this sense, *T. cruzi* infection provokes a substantial decline in mitochondrial membrane potential (51).

Recent studies indicate mitochondrial damage products (mitochondrial ROS production, cytosolic release of mDNA, and the dissipation of mitochondrial membrane potential) as common factors to trigger nucleotide-binding domain and leucine-rich repeat (NLR) pyrin domain containing-3 (NLRP3) inflammasome activation (52, 53). In line with these findings, we observed altered mitochondrial potential with decreased BHI in monocytes from infected individuals. Therefore, the accumulation of damaged mitochondria might give rise to the activation of the NLRP3 inflammasome with the consequent induction of IL-1β production, which would account for the increased levels of this potent inflammatory cytokine observed in plasma from patients with Chagas disease. On the other hand, the release of ATP can also promote inflammasome activation. Here we have also found increased plasmatic ATP levels in *T. cruzi*–infected patients concomitant with higher monocyte expression of CD39 and CD73 ectoenzymes, which are in charge of eATP metabolic degradation to adenosine. Thus, it is plausible that monocytes promote

eATP degradation to dampen the inflammatory microenvironment. In this sense, it was described that ATP promotes HIF-1α expression (54), with the consequent ectonucleotidase upregulation (55).

In vitro studies supported our hypothesis. Glycolysis inhibition of infected PBMCs (obtained from control donors) suppresses the *T. cruzi*–induced inflammatory Mo/Ma profile, diminishing inflammatory cytokine production and increasing IL-10+ cells. Of note, the increased frequency of IL-10+ Mo/Ma could be an indirect effect of glycolysis inhibition and could be the consequence of IL-1β diminution induced by 2-DG. In accordance with our previous observations, which revealed that IL-1β induces NO production (19, 56), 2-DG reduced IL-1β production, and this reduction could lead to lower cellular secretion of NO. In turn, glycolysis inhibition of infected monocytes decreased nitration of lymphocytes, an effect that depends on cell-cell contact. Supporting the in vitro results, the frequency of NO-producing monocytes positively correlated with the percentage of TN+ lymphocytes in peripheral blood samples from control donors and patients. Through well-designed experimental strategies, Koo and coworkers have recently delineated the metabolic regulation of the macrophage response to *T. cruzi*. By studying in vitro assay murine systems, they found that upon infection macrophages maintain a Krebs cycle–linked oxidative metabolism that allows only a partial iNOS activation. Strikingly, the authors observed that IFN-γ treatment led to complete metabolic shutdown of oxidative metabolism and enhanced the glycolytic source of energy availability in infected macrophages. This shift activates the production of optimal NO and ROS levels, dampening the lack of effective microbicidal response (57).

The major achievement of the present work was to establish that glycolysis could be a key factor that sustains the prooxidative monocyte profile in seropositive patients, even in those with the indeterminate (asymptomatic) chronic form of Chagas disease, also known as the "silent" stage. Etiological treatment of Chagas disease is currently based on 2 compounds, nifurtimox and benznidazole, which have substantial activity in congenital and acute *T. cruzi* infections (>95% and 60%–80% of parasitological cures, respectively) (58). However, a major limitation of these drugs is their limited and variable curative activity in the chronic form of the disease, the most prevalent clinical presentation. Even when etiological treatment is clinically recommended, the evidence-based medicine has not been fully validated, and its use in the chronic phase of the disease is still controversial. The effect of benznidazole treatment on patients with Chagas cardiomyopathy was recently reported in a well-conducted Benznidazole Evaluation for Interrupting Trypanosomiasis (BENEFIT) trial (59). After 5 years of follow-up, the results evidence that treatment with benznidazole is unlikely to have a major preventive effect on the progression of heart disease in patients with chronic Chagas disease, even though the parasite load significantly diminished. Although the exact cause-effect relation for cardiomyopathy development has not yet been revealed, the results described in the present work point out that a sustained prooxidative monocyte profile could be accounting for the chronic state described in these patients.

In summary, altogether the results of the present study demonstrate that chronic *T. cruzi* infection sustains monocyte glycolytic metabolism and HIF-1α/NO pathway activation and expands nonclassical circulating monocytes with increased oxidative potential that may induce nitration of CTLs, affecting their functionality. In concert, the described mechanisms could explain the inefficient parasite clearance, concomitant with a sustained inflammatory environment that underlies the characteristic lesions of chronic Chagas disease.

Methods

Subjects and ethics statement. A total of 95 subjects were recruited at the "Hospital Nuestra Señora de la Misericordia," Córdoba, and at the Instituto Nacional de Parasitología "Dr. Mario Fatala Chabén," Buenos Aires, Argentina. *T. cruzi* infection was diagnosed by IHA and ELISA. Subjects with positive results from these 2 tests were considered infected. Patients with chronic Chagas disease (*n* = 40) were evaluated clinically, including electrocardiogram (ECG) and chest x-rays. Subjects were grouped according to the Kuschnir grading system (20). G0 included seropositive individuals having a normal ECG and a normal chest x-ray; G1 comprised seropositive patients with a normal chest x-ray but abnormalities in the ECG; G2 encompassed seropositive patients with ECG abnormalities and heart enlargement as determined by chest x-rays; and G3 involved seropositive patients with ECG abnormalities, heart enlargement, and clinical or radiological evidence of heart failure. The control group (*n* = 55) consisted of age-matched individuals who were serologically negative for *T. cruzi*. All donors with chronic or inflammatory diseases, erythrocyte sedimentation rate greater than 30 mm, or WBC count less than 4000 or greater than 10,000/ mm³ were excluded from the study.

Blood collection. Approximately 15–30 ml of peripheral blood was drawn from each individual. PBMCs were isolated through density gradient centrifugation using Ficoll-Hypaque PLUS (GE Healthcare Bioscience).

T. cruzi lysate. Protein lysate from *T. cruzi* trypomastigotes was obtained by 4 freeze/thaw cycles, which were followed by sonication. In brief, trypomastigotes from the Tulahuen strain were collected from a monolayer of infected Vero cell cultures. After being washed, the parasites were frozen and thawed 4 times. Thereafter, the sample was sonicated and the supernatant of a 12,000-*g* centrifugation was collected and filtered. Protein concentration was determined by Bradford technique.

Monocyte isolation and bioenergetics studies. Monocytes were purified by positive selection from PBMCs using CD14 Microbeads (EasySep, STEMCELL Technologies), following the manufacturer's instructions. Then, 300,000 cells/well were plated in triplicate in XFp cell culture microplates (Seahorse Agilent) precoated with polyethylenimine (MilliporeSigma) and centrifuged (400 *g*) to attach monocytes. RPMI medium was replaced with 180 μl of assay medium (DMEM XF base [MilliporeSigma] supplemented with 2 mM glutamine, pH 7.4) for ECAR measurements or with 175 μl of assay medium (DMEM XF base supplemented with 4 mM glutamine, 5.5 mM D-glucose, and 1 mM pyruvate, pH 7.4) for OCR determination. Plates were kept at 37°C for 45 minutes and loaded into Seahorse XFp extracellular flux analyzer. OCR was determined at the beginning of the assay (basal OCR) and after the sequential addition of 1 μM oligomycin, 1 μM FCCP, and 0.5 μM rotenone plus antimycin A (Agilent). Monocytes titrated with 0.125–2 μM FCCP and 1 μM FCCP rendered the maximum OCR, so this concentration was used for the experiments. Nonmitochondrial OCR was determined after the addition of 0.5 μM rotenone plus antimycin A and subtracted from all other values before calculating the respiratory parameters, as previously described (60). Respiratory parameters were obtained as follows: basal respiration, baseline OCR; respiration driving proton leak, OCR after oligomycin addition; respiration driving ATP synthesis, basal respiration – respiration driving proton leak; maximum respiration, OCR after FCCP addition; and spare respiratory capacity, maximum respiration – basal respiration. Values were expressed as a percentage of OCR corresponding to the last baseline rate (100%). ECAR was determined at the beginning of the assay and after the sequential addition of 10 mM D-glucose, 1 μM oligomycin, and 100 mM 2-DG. Glycolytic parameters were obtained as follows: glycolysis, ECAR after glucose addition – basal ECAR; glycolytic capacity, ECAR after oligomycin addition – basal ECAR; and glycolytic reserve, glycolytic capacity – glycolysis. Values were expressed as a percentage of ECAR corresponding to the last basal rate (100%). Nonglycolytic ECAR was determined after the addition of 100 mM 2-DG and subtracted from all other values before calculating the glycolytic parameters.

The BHI was estimated according to the equation from Chacko, et al. (61): BHI = (spare respiratory capacity × ATP production)/(nonmitochondrial respiration × proton leak).

Ex vivo flow cytometry. Peripheral blood was lysed with ammonium-chloride-potassium (ACK) lysing buffer (Thermo Fisher Scientific) to remove erythrocytes, and cells were blocked with Fc block and stained with anti–CD14-PECy5 (eBioscience; catalog 15-0149-41, clone 61D3), anti–CD16-PECy7 (eBioscience; catalog 25-0168-41, clone CB16), anti–CD39 biotin (BioLegend; catalog 328204, clone 1A), Streptavidin-APC (eBioscience; catalog 17-4317), anti–CD73-PE (BioLegend; catalog 344003, clone A2D), anti–Glut-1-PE (R&D Systems; catalog FAB1418P, clone 202915), anti-nitrotyrosine (anti-TN) rabbit (MilliporeSigma; catalog N 0409), and anti–rabbit Alexa Fluor 647 (Thermo Fisher Scientific, catalog A-21244). To determine HIF-1α expression, cells were permeabilized with Foxp3 staining buffer set (eBioscience) and labeled with anti–HIF-1α rabbit (Abcam; catalog AB51608, clone EP1215Y) followed either by anti–rabbit Alexa Fluor 488 (Thermo Fisher Scientific, catalog A11034) or by anti–rabbit Alexa Fluor 647 (Thermo Fisher Scientific, catalog A21244) antibodies. Data were acquired with an FACSCanto II flow cytometer (Becton Dickinson) and analyzed using FlowJo software (Tree Star Inc.).

ATP quantification. ATP levels were quantified in plasma from individuals by ATP Determination Kit (Invitrogen), according to the manufacturer's instructions. Briefly, samples were incubated with luminescent reaction mix at room temperature for 30 minutes in a 96-well white plate (Greiner Microlon) protected from light. Luminescence was measured at 560 nm in a Synergy 2 Multi-Mode Reader (BioTek). A standard curve was plotted to calculate the ATP concentration and a regression analysis was applied. It is important to stress that plasma samples were separated from formed elements 35 minutes after blood collection.

Measurement of mitochondrial contents. PBMCs were stained with anti–CD14-PECy5 (eBioscience; catalog 15-0149-41, clone 61D3) and anti–CD16-PECy7 (eBioscience; catalog 25-0168-41, clone CB16), and then MitoTracker Green and MitoSpy Orange staining were performed, according to the manufacturer's instructions (BioLegend), and analyzed by flow cytometry.

Intracellular cytokine measurement. PBMCs were cultured with monensin (GolgiStop, 0.6 μl/ml; BD Biosciences), brefeldin A (GolgiPlug, 1 μl/ml; BD Biosciences), and parasite lysate (10 μg/ml) for 16 hours or LPS (100 ng/ml; MilliporeSigma) for 4 hours (62) and stained with anti–CD14-PECy5 (eBioscience; catalog 15-0149-41, clone 61D3) and anti–CD16-PECy7 (eBioscience; catalog 25-0168-41, clone CB16). After staining of surface markers, cells were fixed and made permeable according to the manufacturer's instructions for BD Cytofix/Cytoperm kit (BD Biosciences). Then the cells were stained with anti–IL-1β-FITC (eBioscience; catalog BMS127, clone B-A15), anti–IL-6-PE (Immunotools; catalog 21670064, clone 8C9), and anti–IL-10-APC (BioLegend; catalog 501419, clone JES3-9D7) antibodies and analyzed by flow cytometry.

Measurement of ROS and nitrogen species. ROS and NO production were evaluated using the molecular probes 2′,7′ dichlorodihydrofluorescein diacetate (H2DCF-DA) and DAF-FM DA (10 μM, Molecular Probes), respectively, and analyzed by flow cytometry. After surface staining, the cells were resuspended in 100 μl of RPMI, and 100 μl of 20-μM H2DCF-DA or 100 μl of 20-μM DAF-FM DA was loaded onto cells in clear-bottom, black-walled plates (Thermo Fisher Scientific). Cells were incubated for 30 minutes at 37°C, washed twice with PBS, and then loaded with 300 μl of PBS. Fluorescence of the oxidized product was measured at excitation/emission of 488/520 nm using the FACSCanto II (BD Biosciences). The nitrite/nitrate content, indicative of NO production, was monitored by the Griess reagent assay (63).

Culture of PBMCs and glycolysis inhibition. Vero cell monolayers were infected with *T. cruzi* Tulahuen trypomastigotes for 3 hours, then washed and maintained in RPMI at 37°C in a 5% CO_2 atmosphere. After 7 days, the parasites were collected from the supernatant of infected cells and harvested by centrifugation (4,400 *g* for 10 minutes) and washed in PBS. PBMCs from 8 control donors were seeded at 2.5×10^5 cells/well and treated with 2-DG (11 mM, R&D Systems) or maintained in medium for 1 hour and then washed and cultured with *T. cruzi* Tulahuen trypomastigotes (1:1 rate) for 3 hours; then, the cells were washed. After 24 hours, culture supernatants were evaluated for NO levels and the cells stained with anti–CD14-PECy5 (eBioscience; catalog 15-0149-41, clone 61D3), anti–CD64-APCCy7 (BioLegend; catalog 305026, clone 10.1), anti–CD206 Alexa Fluor 647 (BioLegend; catalog 321116, clone 42050), anti–IL-1β-FITC (eBioscience; catalog BMS127, clone B-A15), anti–IL-6-PE (Immunotools; catalog 21670064, clone 8C9), and anti–IL-10-PECy7 (BioLegend; catalog 501419, clone JES3-9D7) antibodies; anti-TN antibody produced in rabbit (MilliporeSigma; catalog N 0409); and anti–rabbit Alexa Fluor 647 antibody (Thermo Fisher Scientific, catalog A-21244), and NO production was assessed (Molecular Probes; catalog D23842) by flow cytometry.

Transwell coculture assay. PBMCs obtained from buffy coats from healthy donors were diluted 1:2 with supplemented RPMI and layered on Ficoll-Hypaque gradient (MilliporeSigma). Lymphocytes and monocytes were further purified from PBMCs by sorting. To obtain highly purified T lymphocytes and monocytes, PMBCs were labeled with anti-CD3 Alexa Fluor 488 (BD Biosciences catalog 557694, clone UCTH1) and anti–CD14-PECy5 (eBioscience; catalog 15-0149-41, clone 61D3) for 20 minutes at 4°C and sorted using FACS Aria II (Becton Dickinson). Monocytes were seeded in the lower chamber of a 24-well plate (Thermo Fisher Scientific) at a concentration of 500,000 cells/well and were treated with 2-DG (11 mM; R&D Systems) or maintained in medium for 1 hour. The monolayers were washed and monocytes were infected with *T. cruzi* trypomastigotes (1:1 rate) for 3 hours and then washed. CD3+ cells (3.5×10^5 cells/well) were plated on top of the Transwell inserts or directly cocultured with infected monocytes and incubated overnight at 37°C, 5% CO_2, in an incubator (Thermo Fisher Scientific). The cells were then harvested and stained with anti–CD14 PECy5 (eBioscience; catalog 15-0149-41, clone 61D3), anti–CD3 Alexa Fluor 488 (BD; catalog 557694, clone UCTH1), anti–CD8 APCCy7 (BD; catalog 557834, clone SK1), anti–Glut-1 PE (R&D Systems; catalog FAB1418P, clone 202915), rabbit anti-TN (MilliporeSigma; catalog N 0409), and anti–rabbit Alexa Fluor 647 (Thermo Fisher Scientific, catalog A-21244) antibodies, for flow cytometry.

Statistics. Statistical analysis was performed with GraphPad Prism 5.0 software. Student's *t* test (2-tailed in Figures 1, 2, 3, and 4; 1-tailed in Figures 5 and 6) or Mann-Whitney *U* test was used according to data distribution for statistical analysis when 2 independent groups were analyzed. For paired samples, parametric paired *t* test or nonparametric Wilcoxon's test was used, according to data distribution. For comparisons among more than 2 groups, the data obtained were analyzed by 2-way ANOVA with post hoc Tukey's test. Pearson's correlation coefficient was used to evaluate the association between 2 parametric variables. Statistical significance was set at $P < 0.05$.

Study approval. This study was reviewed and approved by the Comité Institucional de Ética de la Investigación en Salud del Adulto, Ministerio de Salud de la Provincia de Córdoba (Act 194/2014) and by

the Comité de Ética del Instituto Nacional de Parasitología "Dr. Mario Fatala Chabén," Buenos Aires, Argentina. All studies were conducted according to the principles expressed in the Declaration of Helsinki. Signed informed consent documents were obtained from each donor included in the study.

Author contributions

LMS and MPA conceived and designed the experiments. LMS, NE, GB, LPQP, PMA, LMV, EACS, and MPA performed the experiments. LMS, NE, GB, LPQP, PMA, LMV, ÁRM, EACS, YHV, LM, MP, and MPA analyzed the data. LPQP, LMV, ÁRM, YHV, and MP were responsible for handling patients and human samples. LMS and MPA wrote the paper.

Acknowledgments

Address correspondence to: Maria Pilar Aoki, Haya de la Torre and Medina Allende, Ciudad Universitaria, CP 5000, Córdoba, Argentina. Phone: 54.351.5353851, ext. 3181; Email: paoki@fcq.unc.edu.ar.

LMS's present address is: Ann Romney Center for Neurologic Diseases, Brigham and Women's Hospital, Harvard Medical School, Boston, Massachusetts, USA.

1. Ziegler-Heitbrock L, et al. Nomenclature of monocytes and dendritic cells in blood. *Blood*. 2010;116(16):e74–e80.
2. Ziegler-Heitbrock L. Blood monocytes and their subsets: established features and open questions. *Front Immunol*. 2015;6:423.
3. Sanmarco LM, Eberhardt N, Ponce NE, Cano RC, Bonacci G, Aoki MP. New insights into the immunobiology of mononuclear phagocytic cells and their relevance to the pathogenesis of cardiovascular diseases. *Front Immunol*. 2017;8:1921.
4. Hayashi M, et al. Induction of glucose transporter 1 expression through hypoxia-inducible factor 1α under hypoxic conditions in trophoblast-derived cells. *J Endocrinol*. 2004;183(1):145–154.
5. Calvert JW, Cahill J, Yamaguchi-Okada M, Zhang JH. Oxygen treatment after experimental hypoxia-ischemia in neonatal rats alters the expression of HIF-1α and its downstream target genes. *J Appl Physiol*. 2006;101(3):853–865.
6. Liu Y, et al. The expression and significance of HIF-1α and GLUT-3 in glioma. *Brain Res*. 2009;1304:149–154.
7. Gabriely G, Wheeler MA, Takenaka MC, Quintana FJ. Role of AHR and HIF-1α in glioblastoma metabolism. *Trends Endocrinol Metab*. 2017;28(6):428–436.
8. Colegio OR, et al. Functional polarization of tumour-associated macrophages by tumour-derived lactic acid. *Nature*. 2014;513(7519):559–563.
9. Everts B, et al. Commitment to glycolysis sustains survival of NO-producing inflammatory dendritic cells. *Blood*. 2012;120(7):1422–1431.
10. Metzen E, Zhou J, Jelkmann W, Fandrey J, Brüne B. Nitric oxide impairs normoxic degradation of HIF-1α by inhibition of prolyl hydroxylases. *Mol Biol Cell*. 2003;14(8):3470–3481.
11. Báez AL, et al. Chronic indeterminate phase of Chagas' disease: mitochondrial involvement in infection with two strains. *Parasitology*. 2013;140(3):414–421.
12. Ribeiro AL, Rocha MO. [Indeterminate form of Chagas disease: considerations about diagnosis and prognosis]. *Rev Soc Bras Med Trop*. 1998;31(3):301–314.
13. Gutierrez FR, Guedes PM, Gazzinelli RT, Silva JS. The role of parasite persistence in pathogenesis of Chagas heart disease. *Parasite Immunol*. 2009;31(11):673–685.
14. Machado FS, et al. Chagas heart disease: report on recent developments. *Cardiol Rev*. 2012;20(2):53–65.
15. Machado FS, Tyler KM, Brant F, Esper L, Teixeira MM, Tanowitz HB. Pathogenesis of Chagas disease: time to move on. *Front Biosci (Elite Ed)*. 2012;4:1743–1758.

16. Marin-Neto JA, Cunha-Neto E, Maciel BC, Simões MV. Pathogenesis of chronic Chagas heart disease. *Circulation*. 2007;115(9):1109–1123.

17. Schijman AG1, et al. *Trypanosoma cruzi* DNA in cardiac lesions of Argentinean patients with end-stage chronic chagas heart disease. *Am J Trop Med Hyg*. 2004;70(2):210–220.

18. Tarleton RL. Parasite persistence in the aetiology of Chagas disease. *Int J Parasitol*. 2001;31(5–6):550–554.

19. Sanmarco LM, et al. IL-6 improves the nitric oxide-induced cytotoxic CD8+ T cell dysfunction in human Chagas disease. *Front Immunol*. 2016;7:626.

20. Kuschnir E, Sgammini H, Castro R, Evequoz C, Ledesma R, Brunetto J. [Evaluation of cardiac function by radioisotopic angiography, in patients with chronic Chagas cardiopathy]. *Arq Bras Cardiol*. 1985;45(4):249–256.

21. Bowser JL, Phan LH, Eltzschig HK. The hypoxia-adenosine link during intestinal inflammation. *J Immunol*. 2018;200(3):897–907.

22. Zimmermann H. 5′-Nucleotidase: molecular structure and functional aspects. *Biochem J*. 1992;285(Pt 2):345–365.

23. Zimmermann H. Extracellular metabolism of ATP and other nucleotides. *Naunyn Schmiedebergs Arch Pharmacol*. 2000;362(4–5):299–309.

24. Skrzeczyñska J, Kobylarz K, Hartwich Z, Zembala M, Pryjma J. CD14+CD16+ monocytes in the course of sepsis in neonates and small children: monitoring and functional studies. *Scand J Immunol*. 2002;55(6):629–638.

25. Zhang JY, et al. Hyper-activated pro-inflammatory CD16 monocytes correlate with the severity of liver injury and fibrosis in patients with chronic hepatitis B. *PLoS One*. 2011;6(3):e17484.

26. Han J, et al. CD14(high)CD16(+) rather than CD14(low)CD16(+) monocytes correlate with disease progression in chronic HIV-infected patients. *J Acquir Immune Defic Syndr*. 2009;52(5):553–559.

27. Shi LZ, et al. HIF1α-dependent glycolytic pathway orchestrates a metabolic checkpoint for the differentiation of TH17 and Treg cells. *J Exp Med*. 2011;208(7):1367–1376.

28. Mascanfroni ID, et al. Metabolic control of type 1 regulatory T cell differentiation by AHR and HIF1-α. *Nat Med*. 2015;21(6):638–646.

29. Tannahill GM, et al. Succinate is an inflammatory signal that induces IL-1β through HIF-1α. *Nature*. 2013;496(7444):238–242.

30. Chacko BK, Zhi D, Darley-Usmar VM, Mitchell T. The Bioenergetic Health Index is a sensitive measure of oxidative stress in human monocytes. *Redox Biol*. 2016;8:43–50.

31. Tal MC, Sasai M, Lee HK, Yordy B, Shadel GS, Iwasaki A. Absence of autophagy results in reactive oxygen species-dependent amplification of RLR signaling. *Proc Natl Acad Sci U S A*. 2009;106(8):2770–2775.

32. Lu T, Gabrilovich DI. Molecular pathways: tumor-infiltrating myeloid cells and reactive oxygen species in regulation of tumor microenvironment. *Clin Cancer Res*. 2012;18(18):4877–4882.

33. Nagaraj S, Gabrilovich DI. Tumor escape mechanism governed by myeloid-derived suppressor cells. *Cancer Res*. 2008;68(8):2561–2563.

34. Nagaraj S, Schrum AG, Cho HI, Celis E, Gabrilovich DI. Mechanism of T cell tolerance induced by myeloid-derived suppressor cells. *J Immunol*. 2010;184(6):3106–3116.

35. Antonelli LR, et al. The CD14+CD16+ inflammatory monocyte subset displays increased mitochondrial activity and effector function during acute Plasmodium vivax malaria. *PLoS Pathog*. 2014;10(9):e1004393.

36. Mukherjee R, Kanti Barman P, Kumar Thatoi P, Tripathy R, Kumar Das B, Ravindran B. Non-classical monocytes display inflammatory features: validation in sepsis and systemic lupus erythematous. *Sci Rep*. 2015;5:13886.

37. Palmer CS, et al. Glucose transporter 1-expressing proinflammatory monocytes are elevated in combination antiretroviral therapy-treated and untreated HIV+ subjects. *J Immunol*. 2014;193(11):5595–5603.

38. Pérez-Mazliah DE, et al. Distinct monocyte subset phenotypes in patients with different clinical forms of chronic Chagas disease and seronegative dilated cardiomyopathy. *PLoS Negl Trop Dis*. 2018;12(10):e0006887.

39. Dhiman M, et al. Increased myeloperoxidase activity and protein nitration are indicators of inflammation in patients with Chagas' disease. *Clin Vaccine Immunol*. 2009;16(5):660–666.

40. Beltrán B, Mathur A, Duchen MR, Erusalimsky JD, Moncada S. The effect of nitric oxide on cell respiration: A key to understanding its role in cell survival or death. *Proc Natl Acad Sci U S A*. 2000;97(26):14602–14607.

41. Cleeter MW, Cooper JM, Darley-Usmar VM, Moncada S, Schapira AH. Reversible inhibition of cytochrome c oxidase, the terminal enzyme of the mitochondrial respiratory chain, by nitric oxide. Implications for neurodegenerative diseases. *FEBS Lett*. 1994;345(1):50–54.

42. Clementi E, Brown GC, Feelisch M, Moncada S. Persistent inhibition of cell respiration by nitric oxide: crucial role of S-nitrosylation of mitochondrial complex I and protective action of glutathione. *Proc Natl Acad Sci U S A*. 1998;95(13):7631–7636.

43. Ip WKE, Hoshi N, Shouval DS, Snapper S, Medzhitov R. Anti-inflammatory effect of IL-10 mediated by metabolic reprogramming of macrophages. *Science*. 2017;356(6337):513–519.

44. Németh B, et al. Abolition of mitochondrial substrate-level phosphorylation by itaconic acid produced by LPS-induced Irg1 expression in cells of murine macrophage lineage. *FASEB J*. 2016;30(1):286–300.

45. Palsson-McDermott EM, et al. Pyruvate kinase M2 regulates Hif-1α activity and IL-1β induction and is a critical determinant of the Warburg Effect in LPS-activated macrophages. *Cell Metab*. 2015;21(2):347.

46. Van den Bossche J, et al. Mitochondrial dysfunction prevents repolarization of inflammatory macrophages. *Cell Rep*. 2016;17(3):684–696.

47. Mills EL, Kelly B, O'Neill LAJ. Mitochondria are the powerhouses of immunity. *Nat Immunol*. 2017;18(5):488–498.

48. Weinberg SE, et al. Mitochondrial complex III is essential for suppressive function of regulatory T cells. *Nature*. 2019;565(7740):495–499.

49. Guzmán Mentesana G, et al. Functional and structural alterations of cardiac and skeletal muscle mitochondria in heart failure patients. *Arch Med Res*. 2014;45(3):237–246.

50. Vyatkina G, Bhatia V, Gerstner A, Papaconstantinou J, Garg N. Impaired mitochondrial respiratory chain and bioenergetics during chagasic cardiomyopathy development. *Biochim Biophys Acta*. 2004;1689(2):162–173.

51. Gupta S, Bhatia V, Wen JJ, Wu Y, Huang MH, Garg NJ. *Trypanosoma cruzi* infection disturbs mitochondrial membrane potential and ROS production rate in cardiomyocytes. *Free Radic Biol Med*. 2009;47(10):1414–1421.

52. Zhou R, Yazdi AS, Menu P, Tschopp J. A role for mitochondria in NLRP3 inflammasome activation. *Nature*. 2011;469(7329):221–225.

53. Gurung P, Lukens JR, Kanneganti TD. Mitochondria: diversity in the regulation of the NLRP3 inflammasome. *Trends Mol Med*. 2015;21(3):193–201.

54. Amoroso F, Falzoni S, Adinolfi E, Ferrari D, Di Virgilio F. The P2X7 receptor is a key modulator of aerobic glycolysis. *Cell Death Dis*. 2012;3:e370.

55. Eltzschig HK, et al. Coordinated adenine nucleotide phosphohydrolysis and nucleoside signaling in posthypoxic endothelium: role of ectonucleotidases and adenosine A2B receptors. *J Exp Med*. 2003;198(5):783–796.

56. Sanmarco LM, et al. IL-6 promotes M2 macrophage polarization by modulating purinergic signaling and regulates the lethal release of nitric oxide during *Trypanosoma cruzi* infection. *Biochim Biophys Acta Mol Basis Dis*. 2017;1863(4):857–869.

57. Koo SJ, Szczesny B, Wan X, Putluri N, Garg NJ. Pentose phosphate shunt modulates reactive oxygen species and nitric oxide production controlling *Trypanosoma cruzi* in macrophages. *Front Immunol*. 2018;9:202.

58. Urbina JA. Recent clinical trials for the etiological treatment of chronic chagas disease: advances, challenges and perspectives. *J Eukaryot Microbiol*. 2015; 62(1):149–156.

59. Morillo CA, et al. Randomized trial of benznidazole for chronic Chagas' cardiomyopathy. *N Engl J Med*. 2015;373(14):1295–1306.

60. Choi SW, et al. No consistent bioenergetic defects in presynaptic nerve terminals isolated from mouse models of Alzheimer's disease. *J Neurosci*. 2012;32(47):16775–16784.

61. Chacko BK, et al. The Bioenergetic Health Index: a new concept in mitochondrial translational research. *Clin Sci*. 2014;127(6):367–373.

62. Schultz C. Intracytoplasmic detection of proinflammatory cytokines and chemokines in monocytes by flow cytometry. *Methods Mol Biol*. 2003;215:29–39.

63. Tsikas D. Analysis of nitrite and nitrate in biological fluids by assays based on the Griess reaction: appraisal of the Griess reaction in the L-arginine/nitric oxide area of research. *J Chromatogr B Analyt Technol Biomed Life Sci*. 2007;851(1–2):51–70.